

Article

Efficient Removal of Methylene Blue by Bio-Based Sodium Alginate/Lignin Composite Hydrogel Beads

Tao Chen [†], Haochen Liu [†], Jie Gao ^{*†}, Guowen Hu, Yuan Zhao , Xiuqin Tang and Xiaobing Han ^{*†}

Hubei Key Laboratory of Radiation Chemistry and Functional Materials, Non-Power Nuclear Technology, Collaborative Innovation Center, Hubei University of Science and Technology, Xianning 437100, China; taochen518@163.com (T.C.); h2250421565@163.com (H.L.); hgwpublic@163.com (G.H.); zhyf308@hbust.edu.cn (Y.Z.); txqtowd20088@126.com (X.T.)

* Correspondence: gaojie2019@hbust.edu.cn (J.G.); hanxiaobing@hbust.edu.cn (X.H.)

[†] These authors contributed equally to this work.

Abstract: Dye pollution is a serious issue in current environment protection, and bio-based adsorbents have been receiving much attention in wastewater treatment, due to their low cost, renewable, and environmentally friendly characteristics. Bio-based sodium alginate/lignin composite (SA/Lig) hydrogel beads were fabricated by a facile cross-linking with calcium ion and used for the removal of methylene blue (MB). The obtained SA/Lig microbeads were characterized with SEM, FTIR, and TG, and the effect of lignin content, pH, and temperature on the MB adsorption was investigated. The results indicated that the introduction of aromatic lignin can not only enhance thermal stability but also can improve the adsorption performance. Under optimal conditions, the maximum adsorption capacity (254.3 mg/g) was obtained for the SA/Lig-20% beads, with a removal efficiency of 84.8%. The adsorption process for MB is endothermic, and the rate-limiting step is chemical adsorption. The removal efficiency is higher than 90% after five cycles, revealing that the prepared beads show good regeneration ability.



Citation: Chen, T.; Liu, H.; Gao, J.; Hu, G.; Zhao, Y.; Tang, X.; Han, X. Efficient Removal of Methylene Blue by Bio-Based Sodium Alginate/Lignin Composite Hydrogel Beads. *Polymers* **2022**, *14*, 2917. <https://doi.org/10.3390/polym14142917>

Academic Editor: Rajkumar Patel

Received: 3 July 2022

Accepted: 15 July 2022

Published: 19 July 2022

Publisher's Note: MDPI stays neutral with regard to jurisdictional claims in published maps and institutional affiliations.



Copyright: © 2022 by the authors. Licensee MDPI, Basel, Switzerland. This article is an open access article distributed under the terms and conditions of the Creative Commons Attribution (CC BY) license (<https://creativecommons.org/licenses/by/4.0/>).

Keywords: adsorption; sodium alginate; lignin; microbeads; methylene blue

1. Introduction

Nowadays, synthetic dyes have been widely used in the textile industries, leading to serious pollution of water resources [1,2]. Among these dyes, methylene blue (MB) is a commonly used cationic dye, which is more damaging to the environment and humans, as it can be easily combined with negatively charged cell membranes [3,4]. The treatment of MB in wastewater is an urgent issue, and many methods have been developed for the removal of MB. Compared with other methods, adsorption is superior in efficiency and economically [5,6].

To meet the requirements of sustainable development, the renewable, ecofriendly adsorbents originating from biomass were developed for the removal of MB in wastewater. Bio-based lignin-chitosan pellets were fabricated by the Albadarin group [7], and used for the removal of MB, where the maximum adsorption capacity is 36.25 mg/g and the adsorption process can be explained by the pseudo-second-order-model. Marrakchi reported the adsorption of MB with a cross-linked chitosan/sepiolite composite film [8], where the maximum monolayer adsorption capacity is 40.986 mg/g, which was obtained for the CS50SP50 under optimal conditions. Bio-based sodium alginate/soybean extract beads reinforced with hemp hurd and halloysite were reported by Viscusi for the adsorption of MB [9], and the adsorption capacity reached 49 mg/g when adding 35 wt% halloysite. The results of kinetic fitting revealed that the adsorption was based on the chemisorption mechanism. Based on the magnetic separation technology, functional bead adsorbents consisting of iron oxide, activated carbon, and sodium alginate were also reported for the removal of MB [10], and the results showed a maximum adsorption capacity of 222.3 mg/g with a high initial

concentration of 700 mg/L. Recently, covalently cross-linked alginate/montmorillonite composite cryogel with high porosity was reported for the adsorption of MB [11], and the cryogel exhibited effective dye adsorption capacity, where the maximum adsorption capacity against MB was 559.94 mg/g, determined using linear regression of the Langmuir model with an initial concentration of 1000 mg/L.

On the other hand, the intermolecular interaction between the adsorbents and the dye is also an important factor in the design and application [12]. The commercial dyes are aromatic molecules with a negative or positive charge and possess nitrogen or oxygen groups. Based on these features of dyes, electrostatic attraction, π - π stacking, and a hydrogen bond can be designed in the construction of adsorbents. Due to its ionic characteristic, the electrostatic attraction was first taken into account in the adsorbents' design, thus the bio-based positive chitosan and negative cellulose alginate are the most used polymer matrices [7–11]. As the dyes are aromatic molecules, bio-based aromatic tannin- and lignin-based adsorbents have also been developed based on the π - π stacking interaction [13–15]. In addition, the hydrogen bond is another intermolecular interaction involved in the construction of bio-based adsorbents, which can be easily formed between the nitrogen- or oxygen-containing groups in dyes and biomass.

As mentioned above, for the removal of aromatic methylene blue (MB) with nitrogen, bio-based aromatic lignin (Lig) with a hydroxyl group and negative sodium alginate (SA) were used for the adsorbent construction. Bead-type and millimeter-sized SA/Lig composite hydrogel beads were fabricated by a facile cross-linking with calcium ion, and the obtained SA/Lig beads were characterized and used for the removal of MB. The effects of the experimental, thermodynamic, kinetic, and regeneration parameters were also investigated.

2. Materials and Methods

2.1. Materials

Sodium alginate (SA, 200 mPa·s), Lignin (Lig, 96%, Mw = 10,000 g/mol), CaCl₂, and methylene blue (MB, 98%) were purchased from Huaweriruike chemical Co. Ltd. (Beijing, China). Distilled water was used for MB solution preparation.

2.2. Preparation of SA/Lig Composite Hydrogel Beads

The sodium alginate/lignin composite hydrogel beads were prepared as follows [5,6]: Firstly, an amount of lignin was dispersed into 50 mL of water under sonication. Then, 1.0 g of sodium alginate was added to the dispersion at 60 °C under stirring until complete dissolution (the weight percentage of lignin to sodium alginate was 0, 10, 20, 40, 80 wt%). At room temperature, without stirring, the above mixture was added dropwise into a 5 wt% CaCl₂ solution, and the cross-linking reaction was maintained for 24 h. SA/Lig composite beads were obtained with filtration, and then washed with distilled water.

2.3. Characterization of SA/Lig Composite Beads

The surface morphology of the obtained composite beads was determined by scanning electron microscopy (SEM, VEGA-3, Tescan, Czech Republic). The chemical structure of the composites was revealed with Fourier transform infrared (FTIR, Avatar 360 Nicolet instrument). The thermogravimetry (TG) analysis was conducted via a TG 209F3 instrument (NETZSCH Scientific Instruments Ltd., Shanghai, China) under an N₂ atmosphere. The absorbance of the MB solution was determined with an S 3100 spectrophotometer (Mapada Instruments Co., Ltd., Shanghai, China), and the standard curve ($A = 0.182C - 0.017$, and A and C are the absorbance and concentration of MB, respectively) was obtained with the determination of MB absorbance at 664 nm.

2.4. Removal of Methylene Blue

The adsorption of MB from the aqueous solution onto SA/Lig beads was conducted by the batch procedure. Then, 20 mg of dried SA/Lig adsorbents were soaked in 30 mL

of the MB solution, then the solution was placed in an isothermal water bath shaker at 150 rpm. The pH of the solution was adjusted with 0.1 M NaOH and an HCl solution. The concentration of MB was measured using UV-vis spectroscopy at 664 nm [15]. The adsorption capacity Q (mg/g) and removal efficiency R (%) was calculated as follows:

$$Q = (C_i - C_t)V/m \quad (1)$$

$$R = (C_i - C_t) \times 100/C_0 \quad (2)$$

C_i (mg/L) and C_t (mg/L) refer to the MB concentration before and after adsorption, W (g) is the dosage of SA/Lig adsorbents, and V (L) is the volume of the aqueous solution.

3. Results and Discussion

The goal of this work was to reveal the morphology, chemical structure, and thermal stability of the obtained SA/Lig beads, as well as the influence of lignin content, pH, and temperature on the MB adsorption performance. In addition, the thermodynamics, kinetics, and regeneration were also investigated to reveal the adsorption mechanism, thermic effect, and recyclability.

3.1. Fabrication and Characterization of SA/Lig Composite Beads

3.1.1. Surface Morphology

The pictures and surface morphology of pure and SA beads and SA/Lig-20% beads are shown in Figure 1. The obtained composite beads are spherical in shape and show uniform size distribution. The pure SA beads show a colorless and transparent appearance with a diameter of approximately 2 mm, while the color changed to red-brown with a diameter of approximately 1.5 mm for SA/Lig-20% beads. The pure SA beads present a relatively smooth surface similar to the chitosan/gelatin/graphene beads [16], while the SA/Lig beads show a wrinkled morphology with an enhanced surface area, similar to the lignin-containing cellulose nanocrystals/sodium alginate beads [5]. This illustrates that the incorporation of aromatic lignin into the sodium alginate enhances the surface area of the beads, which will benefit the adsorption of MB. These adsorbents are millimeter-sized beads, similar to the commercial macroporous adsorption resin, which will benefit the application in industry [17].

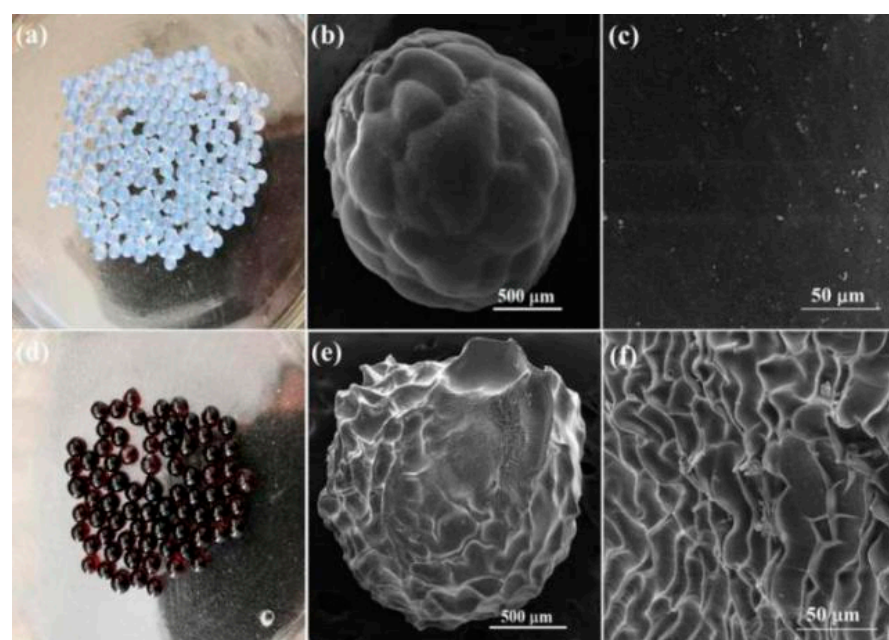


Figure 1. Photos (a) and SEM images (b) $\times 100$, (c) $\times 1000$ of pure SA beads, photos (d) and SEM images (e) $\times 100$, (f) $\times 1000$ of SA/Lig-20% beads.

3.1.2. Composition Analysis

The FTIR spectra of SA, Lig, and SA/Lig-20% beads are shown in Figure 2. In the spectra of SA, the peak at 1029 cm^{-1} is assigned to the stretching of C-O, while the peaks at 1419 and 1625 cm^{-1} are attributed to the symmetric and asymmetric stretching of carboxylate groups [18,19]. For the spectra of Lig, the broad band at 3415 cm^{-1} is ascribed to the -OH group, while the peaks at 1599 and 1443 cm^{-1} refer to the C-C stretching vibration for the aromatic skeleton [5], which is beneficial for the adsorption of MB through the formation of the π - π stacking interaction. For the SA/Lig-20% beads, all the peaks of SA and Lig can be observed, and the symmetric stretching of carboxylate shifts from 1419 to 1425 cm^{-1} , which is consistent with the lignin/sodium alginate composite cross-linked via calcium ion [5,6], demonstrating the formation of SA/Lig composite beads.

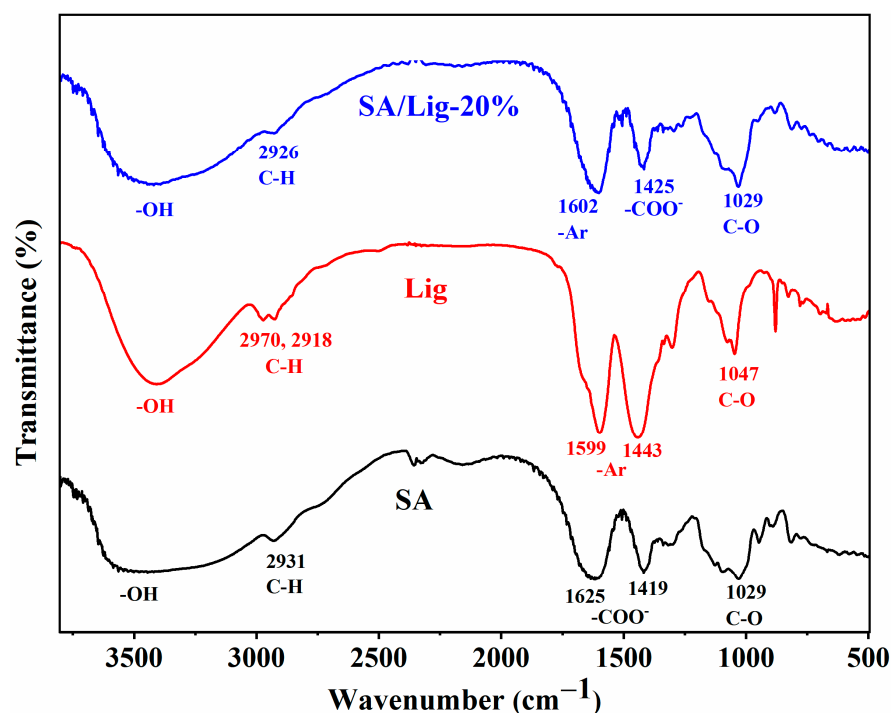


Figure 2. FTIR spectra of SA, Lig, SA/Lig-20% beads.

3.1.3. Thermal Stability

The TG curves of SA, Lig, and SA/Lig-20% beads are shown in Figure 3. Lig shows the highest thermal stability with three degradation steps: The weight loss occurred below $150\text{ }^{\circ}\text{C}$ owing to the loss of the absorbed water; the obvious degradation process at approximately 250 to $400\text{ }^{\circ}\text{C}$ can be associated with the decomposition of oxygen-containing groups and cleaving of C-C bonds; and the last weight loss after $400\text{ }^{\circ}\text{C}$ might be attributed to the degradation of the aromatic structure [20–22]. For the TG curves of SA, the weight loss of absorbed water is approximately 8% before $120\text{ }^{\circ}\text{C}$. In the second stage, the weight loss of approximately 6% between 150 and $230\text{ }^{\circ}\text{C}$ can be ascribed to the decarboxylation of SA. The weight loss between 230 and $450\text{ }^{\circ}\text{C}$ is due to the decomposition of the aminopropyl groups and bisaldehyde, and the organic species have been completely decomposed after $450\text{ }^{\circ}\text{C}$ [10]. For the curve of SA/Lig-20% beads, degradation behavior similar to SA and improved thermal stability were observed for the composite beads, which can be attributed to the incorporation of the rigid structure of aromatic Lig molecules and the calcium ion cross-linking [10,13].

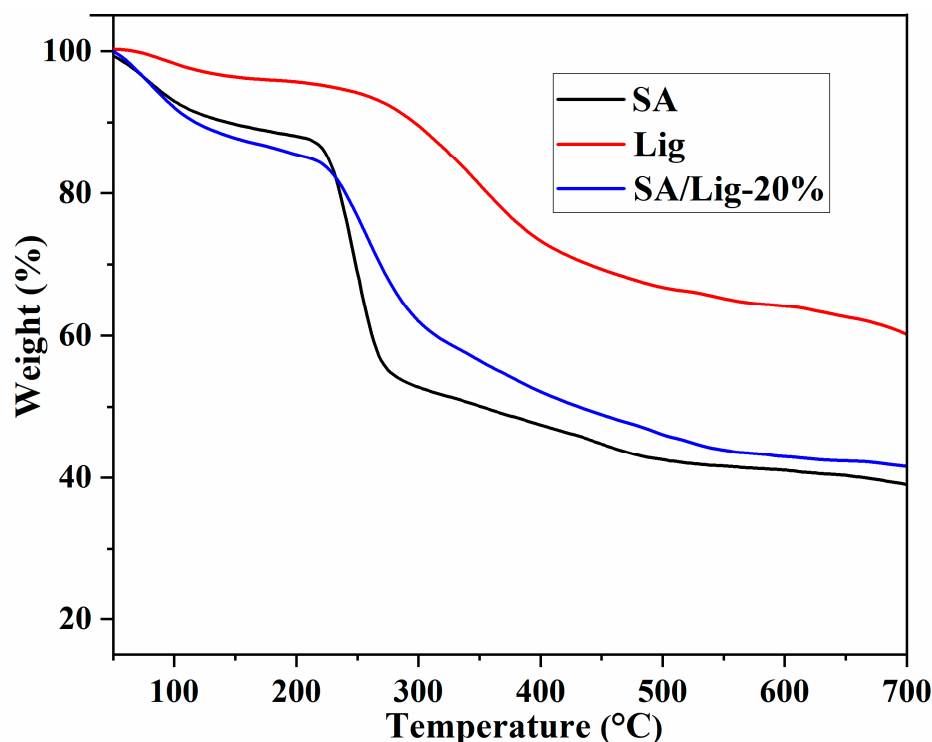


Figure 3. TG spectra of SA, Lig, SA/Lig-20% beads.

3.2. Removal of MB with SA/Lig Beads

3.2.1. Effect of Lignin Content

The adsorption capacity of MB with different SA/Lig beads is shown in Figure 4. With the incorporation of aromatic lignin, the adsorption capacity of the composite beads clearly was enhanced. The maximum adsorption capacity (254.3 mg/g) was observed for the SA/Lig-20% adsorbent, with a removal rate of 84.8%. This is much higher than that of SA beads, which can be attributed to the formation of intermolecular interaction such as π - π stacking and a hydrogen bond between the lignin component and the MB molecules, similar to the adsorption of Congo red onto graphene oxide/chitosan pellets [23,24]. When the content of lignin exceeded 20%, the adsorption capacity decreased, which can be ascribed to the hindered effect of excessive rigid lignin for the diffusion of MB molecules, which is consistent with the results of the lignin/chitosan beads [13] and chitosan/graphene composite spheres [25]. As the highest adsorption capacity was obtained for the SA/Lig-20% beads, these adsorbents were thus chosen for further investigation.

3.2.2. Effect of pH Value

As the pH value is one of the most important parameters that influence the adsorption performance, the effect of the solution pH (4–12) on the adsorption capacity was investigated with SA/Lig-20% beads. As shown in Figure 5, the adsorption capacity shows a high dependence on the pH value, revealing that electrostatic attraction plays an important role in the adsorption of ionic MB. The highest adsorption capacity (240.3 mg/g) was obtained at a pH of 12, with a removal efficiency of 80.1%. This can be attributed to the disadvantage of the high H^+ concentration, which has competitive adsorption with positive MB, and a similar phenomenon was observed in the methylene blue and Congo red removal [13–15]. Taking the protection of the environment and equipment into account, adsorption at a higher pH value (>12) was not conducted.

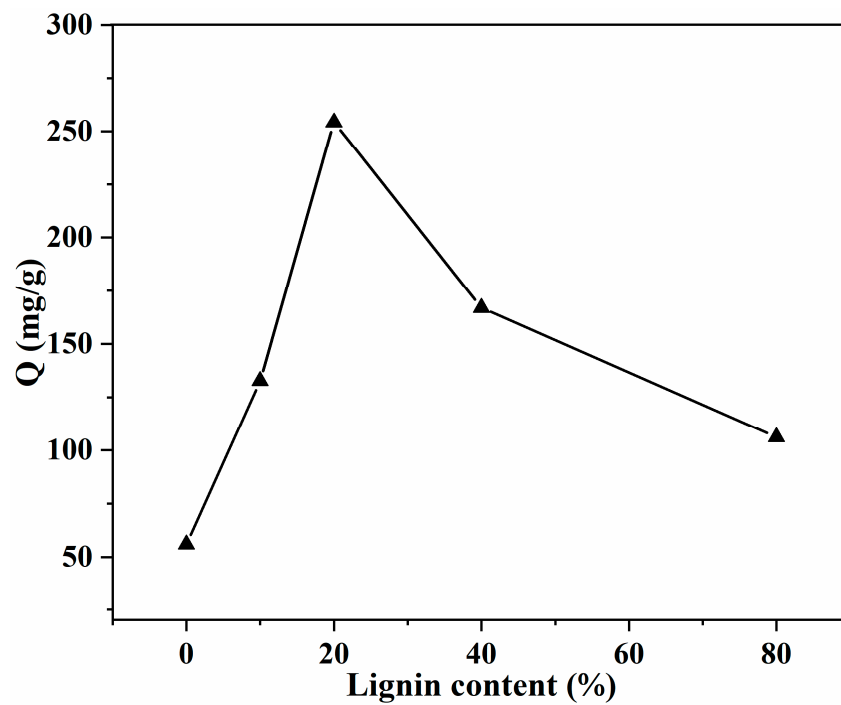


Figure 4. Effect of Lignin content on the adsorption capacity ($m = 20$ mg, $C_0 = 200$ mg/L, $V = 30$ mL, $\text{pH} = 7$, $T = 25$ °C, $s = 150$ r/min, $t = 24$ h).

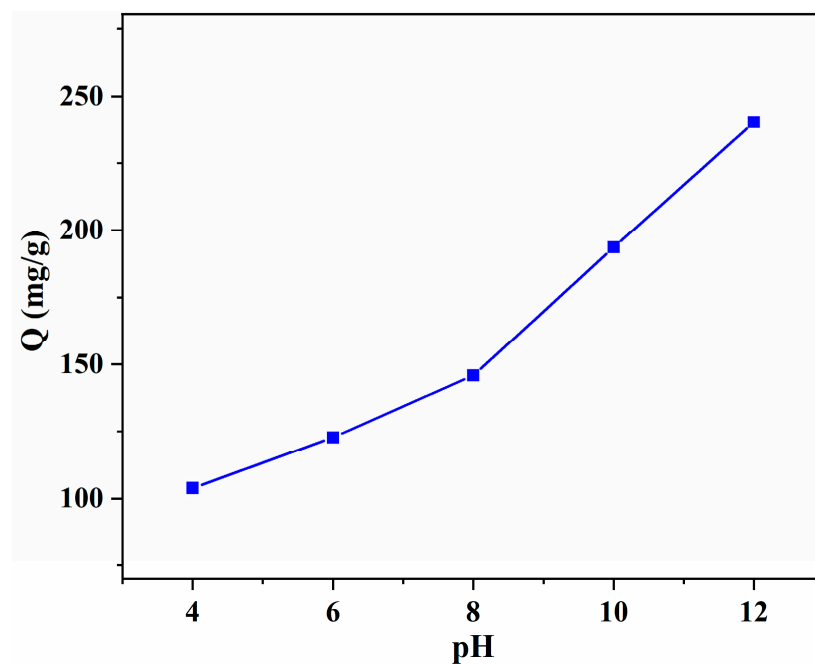


Figure 5. Effect of the pH value on the adsorption capacity with SA/Lig-20% beads ($m = 20$ mg, $C_0 = 200$ mg/L, $V = 30$ mL, $T = 25$ °C, $s = 150$ r/min, $t = 4$ h).

3.3. Adsorption Thermodynamic

The temperature is another significant parameter that can reveal the thermic effect of the adsorption process. The effect of the temperature on the adsorption capacity of the SA/Lig-20% beads is shown in Figure 6. As the temperature increased, the adsorption capacity increased gradually, revealing that adsorption is an endothermic process. This can be ascribed to the increase in the mobility of MB molecules and the number of active sites of the composite adsorbents, which is similar to the adsorption of anionic dye with palm

kernel fibers [26]. The maximum adsorption capacity (256.3 mg/g) was observed at 45 °C, and adsorption at higher temperatures was not conducted as it required more energy.

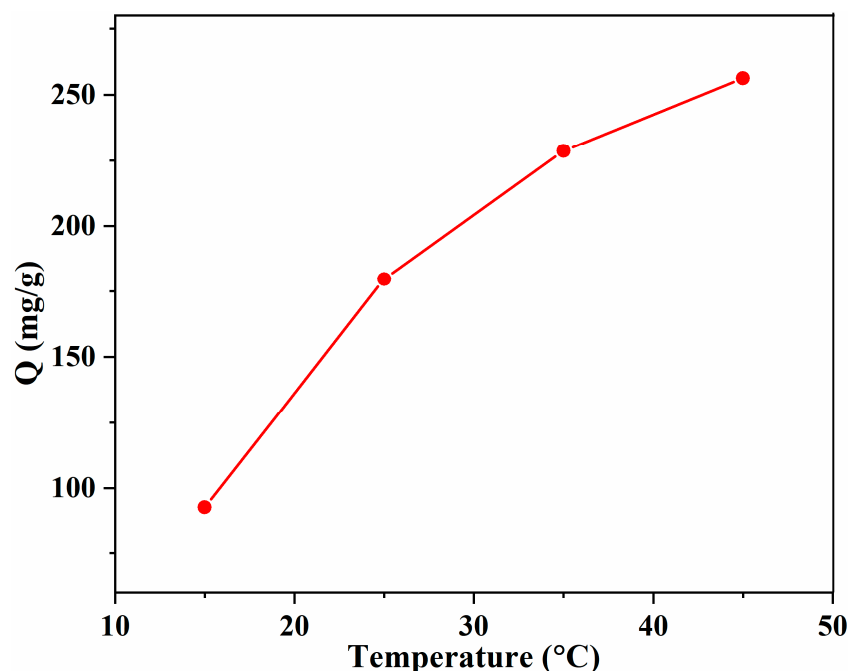


Figure 6. Effect of the temperature on the adsorption capacity with SA/Lig-20% beads ($m = 20$ mg, $C_0 = 200$ mg/L, pH = 12, $s = 150$ r/min, $t = 4$ h).

The thermodynamic parameters including K^0 , ΔG^0 , ΔH^0 , and ΔS^0 can be calculated by the following equations [13,27]:

$$\ln K^0 = \ln(Q_e/C_e) \quad (3)$$

$$\Delta G^0 = -RT \ln K^0 \quad (4)$$

$$R \ln K^0 = -\Delta H^0/T + \Delta S^0 \quad (5)$$

where Q_e is the adsorption capacity, C_e is the equilibrium concentration, R is the universal gas constant (8.314 J/mol·K), and T is the temperature in Kelvin.

The ΔH^0 and ΔS^0 are calculated from the linear plot of $\ln K^0$ versus $1/T$. The calculated parameters are listed in Table 1. With the increase in the temperature, the ΔG^0 decreased dramatically, revealing that an enhanced temperature is favorable for the adsorption, which is consistent with the results mentioned above. When the temperature is 288 K, the value of ΔG^0 is positive, revealing that adsorption cannot proceed spontaneously [15]. With a further increase in the temperature, the value of ΔG^0 changes to negative, indicating adsorption can proceed spontaneously at high temperatures. ΔH^0 and ΔS^0 calculated from the slope and intercept are 64.19 kJ/mol and 0.22 kJ/mol·K, respectively, and the positive value of ΔH^0 demonstrated an endothermic feature of the MB adsorption.

Table 1. Thermodynamic parameters for the adsorption of MB on SA/Lig-20% beads.

Temperature (K)	$\ln K^0$	ΔG^0 (kJ/mol)	ΔH^0 (kJ/mol)	ΔS^0 (kJ/mol·k)
288	−0.805	1.93	64.19	0.22
298	0.398	−0.99	-	-
308	1.166	2.98	-	-
318	1.77	4.68	-	-

3.4. Adsorption Kinetic

The effect of the initial concentration and contact time on the adsorption of MB is shown in Figure 7. As the initial concentration increased, the equilibrium concentration increased, indicating that MB adsorption is dependent on the initial concentration [13]. It will take a long time to diffuse into the adsorbents' matrix for MB molecules after the saturation adsorption, which is similar to the removal of MB with bio-based chitosan microspheres grafted with sodium polystyrene sulfonate [15].

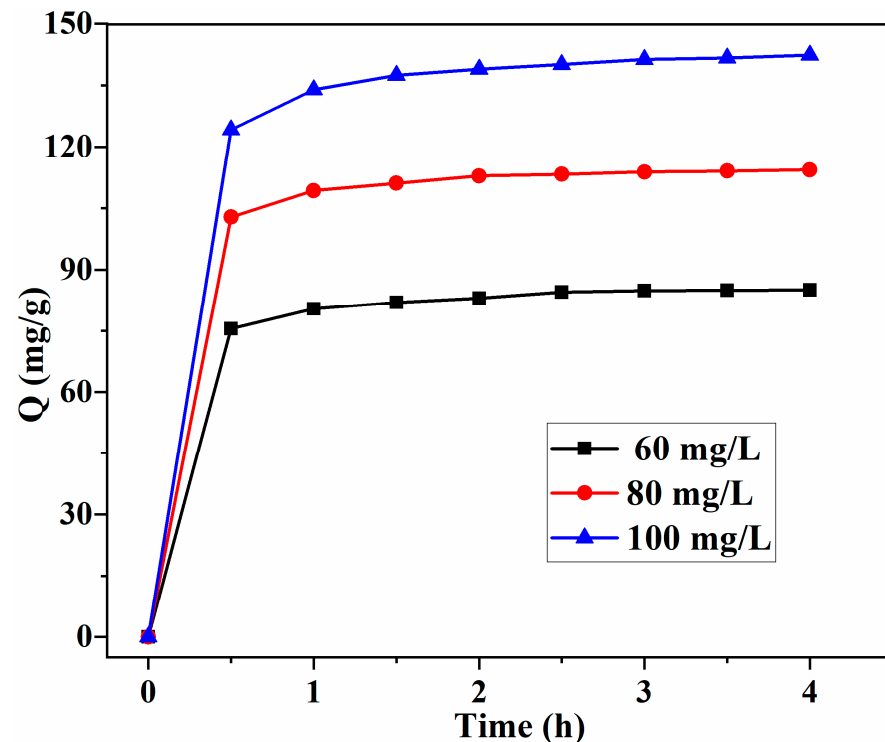


Figure 7. Effect of initial concentration and contact time on the adsorption capacity with SA/Lig-20% beads ($m = 20$ mg, $V = 200$ mL, $\text{pH} = 12$, $T = 45$ °C, $s = 150$ r/min).

The adsorption kinetics can reveal the adsorption mechanism and efficiency and determine the application of the fabricated adsorbents. To provide deeper insight into the adsorption process and mechanism of MB adsorption onto SA/Lig beads, pseudo-first-order and pseudo-second-order kinetic models were used to evaluate the adsorption kinetic (Equations (6) and (7)) [28–33].

Pseudo-first-order:

$$\log(q_e - q_t) = \log q_e - k_1 t \quad (6)$$

Pseudo-second-order:

$$\frac{t}{q_t} = \frac{1}{k_2 q_e^2} + \frac{t}{q_e} \quad (7)$$

where q_e and q_t are the adsorption capacity at equilibrium and time t , respectively, and k_1 and k_2 are the rate constants for the two models.

The fitting curves of the adsorption with different kinetic models are shown in Figure 8, and the calculated parameters are summarized in Table 2. The experimental value is very close to that calculated for the pseudo-second-order model, with the equilibrium adsorption capacity at different initial concentrations. The correlation coefficient R^2 (0.9999) shows that this model fits the experimental data better than that of the pseudo-first-order model, demonstrating that chemical adsorption is the rate-limiting step for the MB molecules adsorption [13,15].

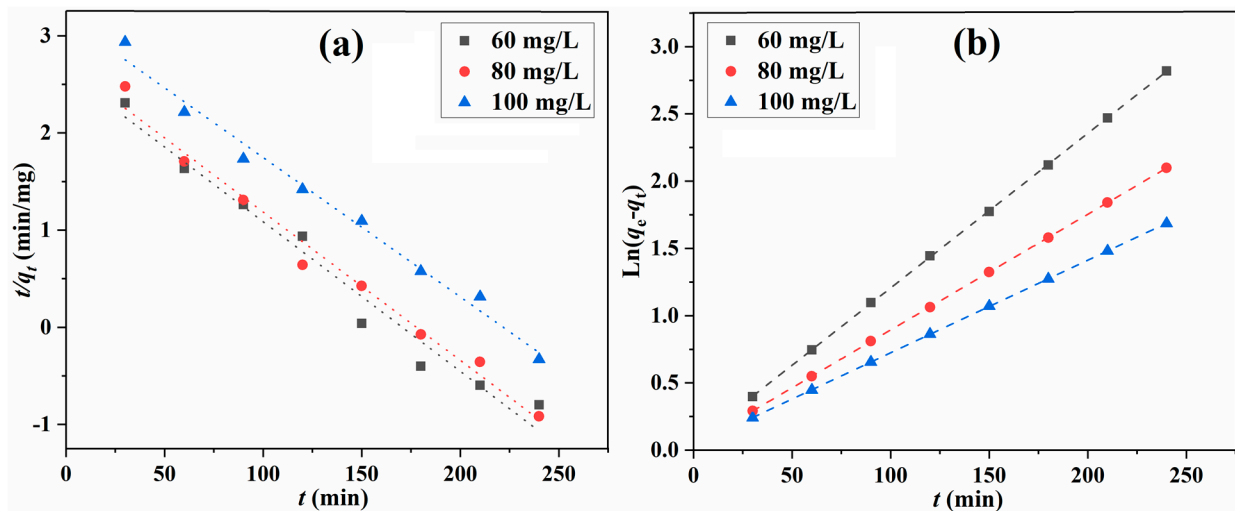


Figure 8. Fitting of pseudo-first-order (a) and pseudo-second-order kinetic (b) models for the adsorption process.

Table 2. Kinetic parameters of two models for MB adsorption.

Kinetic Models	Coefficients	60 mg/L	80 mg/L	100 mg/L
Pseudo-first-order	$q_{e,cal}$ (mg/g)	13.82	15.06	24.05
	k_1 (min^{-1})	0.0154	0.0163	0.0144
	R^2	0.9711	0.9846	0.9871
Pseudo-second-order	$q_{e,cal}$ (mg/g)	87.03	116.28	145.35
	k_2 ($\times 10^{-3}$) (g/mg min)	2.34	2.21	1.32
	R^2	0.9999	0.9999	0.9999

3.5. Regeneration Performance

The regeneration performance is also an important factor for the adsorbents, therefore the regeneration behavior of the obtained SA/Lig beads was evaluated with the desorption experiment. The desorption of MB from SA/Lig-20% beads was realized with a 1 M HCl aqueous solution in an incubator shaker, washed with distilled water. As shown in Figure 9, the removal efficiency decreased slightly but was still higher than 90% after five cycles, at which point the adsorption capacity decreased from 14.55 mg/g to 13.80 mg/g, revealing that the obtained SA/Lig beads have a good regeneration ability [13,15]. This is much better than the MB removal with Kaolin [32], with a removal efficiency that decreased from 56% to 23% after four cycles.

3.6. Adsorption Performance Comparison

The maximum adsorption capacity, removal efficiency, and regeneration of the obtained SA/Lig beads were compared with bio-based materials in the literature [34,35]. As shown in Table 3, there are almost no regeneration data for the reported adsorbents [7–11]. Though some of the adsorbents show a much high adsorption capacity at a high initial concentration, the removal efficiency is relatively low. The SA/Lig beads show a relatively high adsorption capacity and removal efficiency compared to most similar bio-based adsorbents, and the improved adsorption performance can be attributed to the combination of aromatic lignin with SA [13,14].

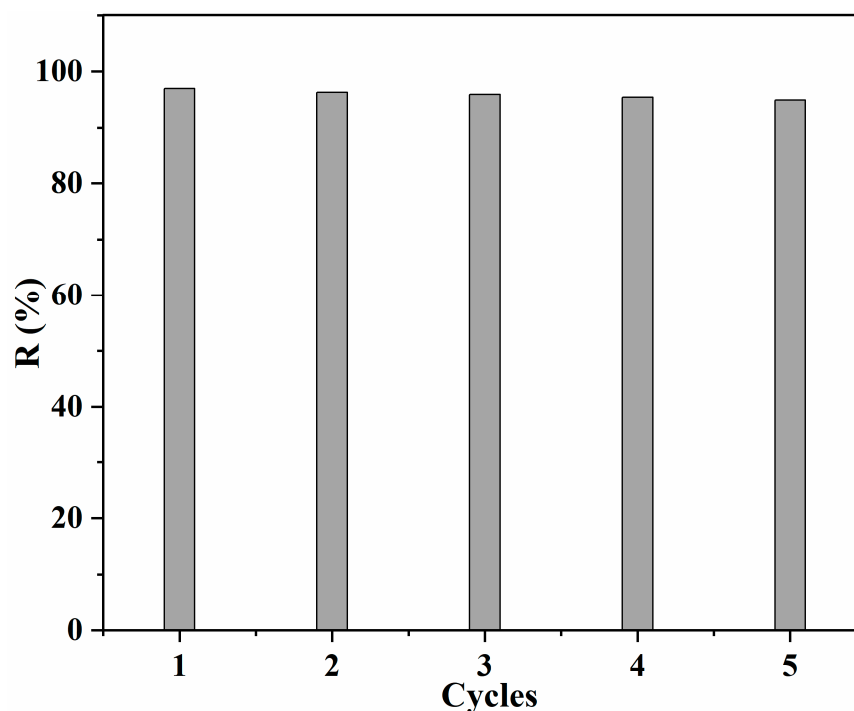


Figure 9. Effect of recycling times on the adsorption capacity Q (mg/g) with 40%Tan/SA beads ($m = 20$ mg, $C_0 = 10$ mg/L, $V = 30$ mL, $\text{pH} = 12$, $T = 45$ °C, $s = 150$ r/min, $t = 4$ h).

Table 3. Comparison of the MB removal performance with similar adsorbents.

Adsorbent	Experimental Conditions (C_0 /(mg/L), pH, T/°C, t/h)	Q_{max} (mg/g)	Removal (%)	Ref.
SA/Lig	200, 12, 45, 24	254.3	84.8	This work
Lig/CS	82, 7, 20, 40	36.25	88.4	[7]
CS/SP	300, 9, 30, 24	40.986	27.3	[8]
SA/SB/HNT	100, 7, 25, 24	49	94	[9]
Fe ₃ O ₄ /AC/SA	700, 7, 25, 4	222.3	31.8	[10]
SA/MMT	1000, 7, 25, 24	559.94	56	[11]

4. Conclusions

In summary, bio-based sodium alginate/lignin composite hydrogel beads were fabricated by facile cross-linking with calcium ions and were used for the efficient removal of methylene blue. The incorporation of aromatic lignin into sodium alginate not only improved the thermal stability of the obtained adsorbents but also enhanced the adsorption performance. The maximum adsorption capacity of 254.3 mg/g (removal efficiency of 84.8%) was obtained for SA/Lig-20%, under the optimal conditions of $\text{pH} = 12$, $T = 45$ °C. The calculated thermodynamic and kinetic parameters revealed that adsorption is an endothermic process, and chemical adsorption is the rate-limiting step. In addition, the obtained adsorbents show a good regeneration ability. The prepared SA/Lig composite beads have promising applications for the removal of cationic dyes from wastewater, and future work will focus on the selectivity, scale-up, and continuous column adsorption of these adsorbents.

Author Contributions: Experiment design, J.G. and T.C.; sample preparation, X.H., H.L. and X.T.; structure characterization, X.H., Y.Z. and X.T.; property analysis, H.L., Y.Z. and G.H.; writing—original draft, J.G.; review and editing, T.C. and G.H.; supervision, T.C.; project administration, J.G. All authors have read and agreed to the published version of the manuscript.

Funding: This research was funded by National Natural Science Foundation of China (51903080), the Innovation and Entrepreneurship Training Program for College Students of Hubei Province (S202210927005), the Innovation Team of Hubei University of Science and Technology (2022T03), and the Scientific Research Foundation of Hubei University of Science and Technology (BK202003, 2021ZX15).

Institutional Review Board Statement: Not applicable.

Informed Consent Statement: Not applicable.

Data Availability Statement: Not applicable.

Conflicts of Interest: The authors declare no conflict of interest.

References

1. Sala, E.; Mayorga, J.; Bradley, D.; Cabral, R.B.; Atwood, T.B.; Auber, A.; Cheung, W.; Costello, C.; Ferretti, F.; Friedlander, A.M.; et al. Protecting the global ocean for biodiversity, food and climate. *Nature* **2021**, *7854*, 397–402. [[CrossRef](#)]
2. Sullivan, S.M.P.; Rains, M.C.; Rodemald, A.D.; Buzbee, W.W.; Rosemond, A.D. Distorting science, putting water at risk. *Science* **2020**, *6505*, 766–768. [[CrossRef](#)] [[PubMed](#)]
3. Singh, K.P.; Gupta, S.; Singh, A.K.; Sinha, S. Optimizing adsorption of crystal violet dye from water by magnetic nano composite using response surface modeling approach. *J. Hazard. Mater.* **2011**, *186*, 1462–1473. [[CrossRef](#)] [[PubMed](#)]
4. Roosta, M.; Ghaedi, M.; Daneshfar, A.; Sahraei, R.; Asghari, A. Optimization of the ultrasonic assisted removal of methylene blue by gold nanoparticles loaded on activated carbon using experimental design methodology. *Ultrason. Sonochem.* **2014**, *21*, 242–252. [[CrossRef](#)]
5. Ma, M.S.; Liu, Z.; Hui, L.F.; Shang, Z.; Yuan, S.Y.; Dai, L.; Liu, P.T.; Liu, X.L.; Ni, Y.H. Lignin-containing cellulose nanocrystals/sodium alginate beads as highly effective adsorbents for cationic organic dyes. *Int. J. Biol. Macromol.* **2019**, *139*, 640–646. [[CrossRef](#)] [[PubMed](#)]
6. Mohammadabadi, S.I.; Javanbakht, V. Lignin extraction from barley straw using ultrasound-assisted treatment method for a lignin-based biocomposite preparation with remarkable adsorption capacity for heavy metal. *Int. J. Biol. Macromol.* **2020**, *164*, 1133–1148. [[CrossRef](#)] [[PubMed](#)]
7. Albadarin, A.; Collins, M.N.; Naushad, M.; Shirazian, S.; Walker, G.; Mangwandi, C. Activated lignin-chitosan extruded blends for efficient adsorption of methylene blue. *Chem. Eng. J.* **2017**, *307*, 264–272. [[CrossRef](#)]
8. Marrakchi, F.; Khanday, W.A.; Asif, M.; Hameed, B.H. Cross-linked chitosan/sepiolite composite for the adsorption of methylene blue and reactive orange 16. *Int. J. Biol. Macromol.* **2016**, *93*, 1231–1239. [[CrossRef](#)]
9. Viscusi, G.; Lamberti, E.; Gorrasi, G. Design of sodium alginate/soybean extract beads loaded with hemp hurd and halloysite as novel and sustainable systems for methylene blue adsorption. *Polym. Eng. Sci.* **2022**, *62*, 129–144. [[CrossRef](#)]
10. Li, C.D.; Lu, J.J.; Li, S.M.; Tong, Y.B.; Ye, B.C. Synthesis of magnetic microspheres with sodium alginate and activated carbon for removal of methylene blue. *Materials* **2017**, *10*, 84. [[CrossRef](#)]
11. Sezen, S.; Thakur, V.K.; Ozmen, M.M. Highly effective covalently crosslinked composite alginate cryogels for cationic dye removal. *Gels* **2021**, *7*, 178. [[CrossRef](#)] [[PubMed](#)]
12. Villarreal, I.A.; Arriagada, D.C.; Mayorga, C.K.; Urbina, K.P.; Valencia, R.M.; Gonzalez, J. Importance of the interaction adsorbent-adsorbate in the dyes adsorption process and DFT modeling. *J. Mol. Struct.* **2020**, *1203*, 127398. [[CrossRef](#)]
13. Han, X.B.; Li, R.; Miao, P.P.; Gao, J.; Hu, G.W.; Zhao, Y.; Chen, T. Design, synthesis and adsorption evaluation of bio-based lignin/chitosan beads for congo red removal. *Materials* **2022**, *15*, 2310. [[CrossRef](#)] [[PubMed](#)]
14. Hu, T.; Liu, Q.Z.; Gao, T.T.; Dong, K.J.; Wei, G.; Yao, J.S. Facile preparation of tannic acid-poly(vinyl alcohol)/sodium alginate hydrogel beads for methylene blue removal from simulated solution. *ACS Omega* **2018**, *3*, 7523–7531. [[CrossRef](#)]
15. Chen, T.; Zhao, Y.; Sang, Y.N.; Tang, M.; Hu, G.W.; Han, X.B.; Gao, J.; Ma, R. Facile synthesis of magnetic CS-g-SPSS microspheres via electron beam radiation for efficient removal of methylene blue. *J. Saudi Chem. Soc.* **2021**, *25*, 101299. [[CrossRef](#)]
16. Wu, M.; Chen, W.J.; Mao, Q.H.; Bai, Y.S.; Ma, H.Z. Facile Synthesis of chitosan/gelatin filled with graphene bead adsorbent for orange II removal. *Chem. Eng. Res. Des.* **2019**, *144*, 35–46. [[CrossRef](#)]
17. Duan, Y.Q.; Freyburger, A.; Kunz, W.; Zollfrank, C. Lignin/chitin films and their adsorption characteristics for heavy metal ions. *ACS Sustain. Chem. Eng.* **2018**, *6*, 6965–6973. [[CrossRef](#)]
18. Larosa, C.; Salerno, M.; Lima, J.S.; Meri, R.M.; Silva, M.F.; Carvalho, L.B.; Converti, A. Characterisation of bare and tannase-loaded calcium alginate beads by microscopic, thermogravimetric, FTIR and XRD analyses. *Int. J. Biol. Macromol.* **2018**, *115*, 900–906. [[CrossRef](#)]
19. Abulateefeh, S.R.; Taha, M.O. Enhanced drug encapsulation and extended release profiles of calcium-alginate nanoparticles by using tannic acid as a bridging cross-linking agent. *J. Microencapsul.* **2015**, *32*, 96–105. [[CrossRef](#)]
20. Schneider, M.; Finimundi, N.; Podzorova, M.; Pantyukhov, P.; Poletto, M. Assessment of morphological, physical, thermal, and thermal conductivity properties of polypropylene/lignosulfonate blends. *Materials* **2021**, *14*, 543. [[CrossRef](#)]

21. Abboud, M.; Sahlabji, T.; Haija, M.A.; Zahhar, A.A.; Bondock, S.; Ismail, I.; Keshk, S. Synthesis and characterization of lignosulfonate/amino-functionalized SBA-15 nanocomposites for the adsorption of methylene blue from wastewater. *New J. Chem.* **2020**, *44*, 2291–2302. [[CrossRef](#)]
22. Chupin, L.; Charrier, B.; Pizzi, A.; Perdomo, A.; Bouhtoury, F. Study of thermal durability properties of tannin-lignosulfonate adhesives. *J. Therm. Anal. Calorim.* **2015**, *119*, 1577–1585. [[CrossRef](#)]
23. Bai, H.J.; Chen, J.H.; Zhou, X.Y.; Hu, C.Z. Single and binary adsorption of dyes from aqueous solutions using functionalized microcrystalline cellulose from cotton fiber. *Korean J. Chem. Eng.* **2020**, *37*, 1926–1932. [[CrossRef](#)]
24. Du, Q.; Li, Y.; Li, J.; Zhang, Z.; Qiao, B.; Sui, K.; Wang, D.; Wang, C.; Li, H.; Xia, Y.; et al. Preparation of graphene oxide/chitosan pellets and their adsorption properties for congo red. *Int. J. Nanosci.* **2019**, *18*, 1850030. [[CrossRef](#)]
25. Zhang, C.L.; Chen, Z.Z.; Guo, W.; Zhu, C.W.; Zou, Y.J. Simple fabrication of chitosan/graphene nanoplates composite spheres for efficient adsorption of acid dyes from aqueous solution. *Int. J. Biol. Macromol.* **2018**, *112*, 1048–1054. [[CrossRef](#)]
26. Ofomaja, A.E.; Ho, Y.S. Equilibrium sorption of anionic dye from aqueous solution by palm kernel fibre as sorbent. *Dye Pigment.* **2007**, *74*, 60–66. [[CrossRef](#)]
27. Zhang, L.J.; Zhao, D.Q.; Lu, Y.; Chen, J.H.; Li, H.T.; Xie, J.H.; Xu, Y.; Yuan, H.K.; Liu, X.J.; Zhu, X.Y.; et al. A Graphene oxide modified cellulose nanocrystal/PNIPAAm IPN hydrogel for the adsorption of congo red and methylene blue. *New J. Chem.* **2021**, *45*, 16679–16688. [[CrossRef](#)]
28. Sartape, A.S.; Mandhare, A.M.; Salvi, P.P.; Pawar, D.K.; Kolekar, S.S. Kinetic and equilibrium studies of the adsorption of Cd(II) from aqueous solutions by wood apple shell activated carbon. *Desalin. Water Treat.* **2013**, *51*, 4638–4650. [[CrossRef](#)]
29. Chen, T.; Yan, C.J.; Wang, Y.X.; Tang, C.H.; Zhou, S.; Zhao, Y.; Ma, R.; Duan, P. Synthesis of activated carbon-based amino phosphonic acid chelating resin and its adsorption properties for Ce(III) removal. *Environ. Technol.* **2015**, *36*, 2168–2176. [[CrossRef](#)]
30. Eldin, M.S.M.; Soliman, E.A.; Elzattahy, A.A.F.; Elaassar, M.R.; Eweida, B.Y.; Elkady, M.F.; Rahman, A.M.A.; Yossef, M.E. Carboxylated alginate hydrogel beads for methylene blue removal: Formulation, kinetic and isothermal studies. *Desalin. Water Treat.* **2019**, *168*, 308–323. [[CrossRef](#)]
31. Uyar, G.; Kaygusuz, H.; Erim, F.B. Methylene blue removal by alginate–clay quasi-cryogel beads. *React. Funct. Polym.* **2016**, *106*, 1–7. [[CrossRef](#)]
32. Mouni, L.; Belkhir, L.; Bollinger, J.C.; Bouzaza, A.; Assadi, A.; Tirri, A.; Dahmoune, F.; Madani, K.; Remini, H. Removal of methylene blue from aqueous solutions by adsorption on Kaolin: Kinetic and equilibrium studies. *Appl. Clay Sci.* **2018**, *153*, 38–45. [[CrossRef](#)]
33. Liu, X.J.; Li, M.F.; Singh, S.K. Manganese-modified lignin biochar as adsorbent for removal of methylene blue. *J. Mater. Res. Technol.* **2021**, *12*, 1434–1445. [[CrossRef](#)]
34. Sabbagh, F.; Muhamad, I.I.; Pa'e, N.; Hashim, Z. Strategies in improving properties of cellulose-based hydrogels for smart applications. In *Cellulose-Based Superabsorbent Hydrogels*; Mondal, M.I.H., Ed.; Springer: Cham, Switzerland, 2019; pp. 887–908.
35. Sabbagh, F.; Muhamad, I.I.; Nazari, Z.; Mobini, P.; Khatir, N.M. Investigation of acyclovir-loaded, acrylamide-based hydrogels for potential use as vaginal ring. *Mater. Today Commun.* **2018**, *16*, 274–280. [[CrossRef](#)]